JCI The Journal of Clinical Investigation

Atrial natriuretic peptide promotes uterine decidualization and a TRAIL-dependent mechanism in spiral artery remodeling

Wei Zhang, Shuo Li, Jinglei Lou, Hui Li, Meng Liu, Ningzheng Dong, Qingyu Wu

J Clin Invest. 2021;131(20):e151053. https://doi.org/10.1172/JCI151053.

Research Article | Vascular biology

Graphical abstract

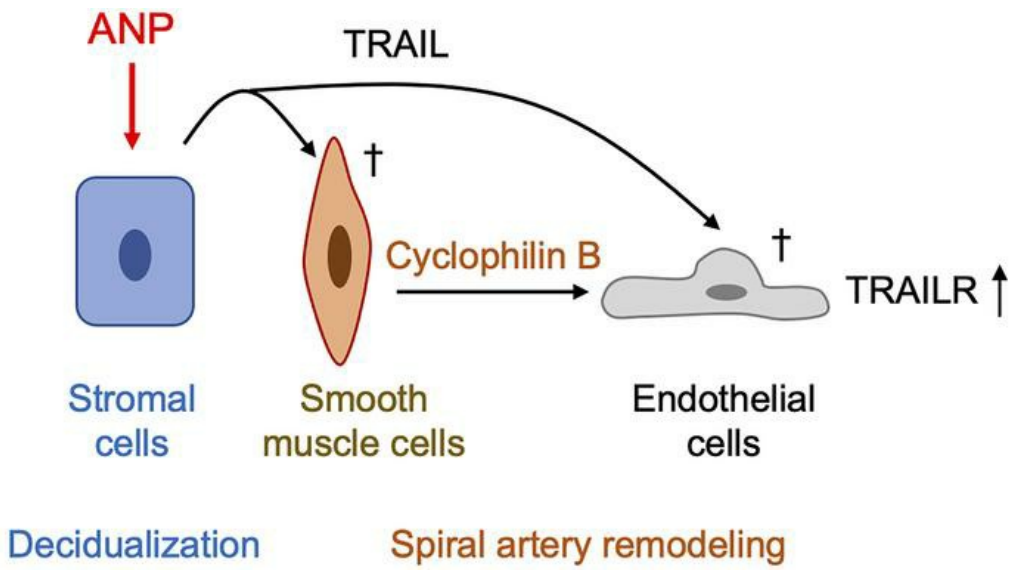

Atrial natriuretic peptide promotes uterine decidualization and a TRAIL-dependent mechanism in spiral artery remodeling

Wei Zhang,[1] Shuo Li,[1] Jinglei Lou,[1] Hui Li,[2] Meng Liu,[3] Ningzheng Dong,[3] and Qingyu Wu[1,3]

[1]Cardiovascular & Metabolic Sciences, Lerner Research Institute, Cleveland Clinic, Cleveland, Ohio, USA. [2]Central Laboratory and Department of Obstetrics and Gynecology, Affiliated Suzhou Hospital of Nanjing Medical University, Suzhou Municipal Hospital, Suzhou, China. [3]Cyrus Tang Hematology Center, Collaborative Innovation Center of Hematology, State Key Laboratory of Radiation Medicine and Prevention, Soochow University, Suzhou, China.

Atrial natriuretic peptide (ANP) is an important hormone in cardiovascular biology. It is activated by the protease corin. In pregnancy, ANP and corin promote uterine spiral artery remodeling, but the underlying mechanism remains unknown. Here we report an ANP function in uterine decidualization and TNF-related apoptosis-inducing ligand–dependent (TRAIL-dependent) death in spiral arterial smooth muscle cells (SMCs) and endothelial cells (ECs). In ANP- or corin-deficient mice, uterine decidualization markers and TRAIL expression were decreased, whereas in cultured human endometrial stromal cells (HESCs), ANP increased decidualization and TRAIL expression. In uterine spiral arteries from pregnant wild-type mice, SMC and EC loss occurred sequentially before trophoblast invasion. In culture, TRAIL from decidualized HESCs induced apoptosis in uterine SMCs, but not in ECs with low TRAIL receptor expression. Subsequently, cyclophilin B was identified from apoptotic SMCs that upregulated endothelial TRAIL receptor and caused apoptosis in ECs. These results indicate that ANP promotes decidualization and TRAIL expression in endometrial stromal cells, contributing to sequential events in remodeling of spiral arteries, including SMC death and cyclophilin B release, which in turn induces TRAIL receptor expression and apoptosis in ECs.

Introduction

Uterine spiral artery remodeling is an adaptive process in pregnancy, during which smooth muscle cells (SMCs) in the vessel wall are lost and luminal endothelial cells (ECs) are replaced by invading placental trophoblasts (1, 2). This vascular remodeling process results in rheological and physiological changes that are essential for steady uteroplacental blood flow with reduced velocity to support the growing fetus (3). Preeclampsia, characterized by hypertension and proteinuria in pregnancy, is a major disease that increases the risk of maternal and fetal mortality (2, 4, 5). A defective uteroplacental interface and impaired spiral artery remodeling play a central role in the pathogenesis of preeclampsia (4, 6–8).

Decidualization, a transforming event in the pregnant uterus, plays a critical role in spiral artery remodeling (9). It occurs before placental trophoblast invasion (10–12). Defective decidualization has been associated with impaired spiral artery remodeling and preeclampsia (13–15). In preeclamptic women, low plasma levels of insulin growth factor–binding protein-1 (IGFBP1), a decidualization marker, have been reported (14). In culture, endometrial stromal cells from preeclamptic women often fail to respond to decidualization induction (15). Gene profiling studies have also revealed poor decidualization in uterine tissues from preeclamptic women (15, 16). It remains unclear, however, how decidualization and spiral artery remodeling are coordinated at the molecular and cellular levels.

Atrial natriuretic peptide (ANP) is a hormone that regulates salt-water balance and vascular homeostasis (17–21). ANP is synthesized as a precursor that is converted to active ANP by corin, a transmembrane serine protease (22–24). In mice, corin deficiency abolishes ANP activation (25, 26). Both corin and ANP are expressed in the pregnant uterus (27–31). In mice, corin or ANP deficiency impairs trophoblast invasion and spiral artery remodeling, leading to a preeclampsia-like phenotype (27, 28, 32). *CORIN* variants impairing corin function have been identified in preeclamptic women (27, 33, 34). To date, how the corin/ANP pathway regulates spiral artery remodeling in the pregnant uterus has not been elucidated.

In this study, we used mouse models to investigate the role of ANP in decidualization during pregnancy. We also conducted series of biochemical and functional experiments in cultured human endometrial stromal cells (HESCs) and uterine SMCs and ECs to understand the mechanism underlying the interplay among those cells. Our results reveal an important role of ANP in regulating sequential molecular and cellular events in decidualization and spiral artery remodeling in the pregnant uterus.

Results

Uterine decidualization is impaired in Nppa$^{-/-}$ and Corin$^{-/-}$ mice. We analyzed 2 decidualization markers, uterine prolactin and IGFBP1 (35), in *Nppa*$^{-/-}$ mice, in which the *Nppa* gene (encoding

Conflict of interest: The authors have declared that no conflict of interest exists.

Submitted: May 4, 2021; **Accepted:** September 1, 2021; **Published:** October 15, 2021.
Reference information: *J Clin Invest*. 2021;131(20):e151053.
https://doi.org/10.1172/JCI151053.

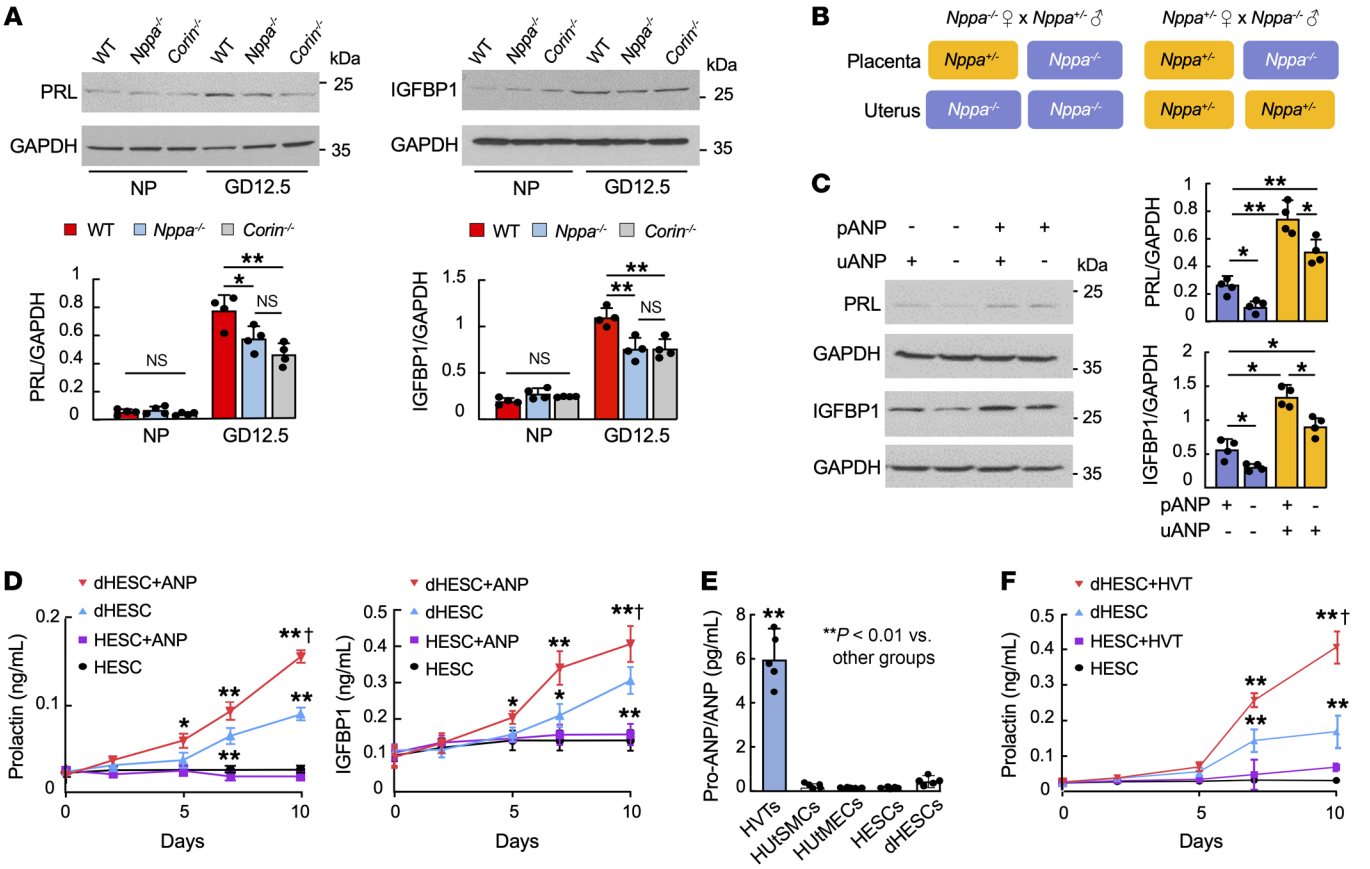

Figure 1. ANP promotes decidualization in pregnant mice and cultured HESCs. (**A**) Western blotting of prolactin (PRL) and IGFBP1 in uteri from non-pregnant (NP) and pregnant (GD12.5) WT, *Nppa*$^{-/-}$, and *Corin*$^{-/-}$ mice. GAPDH was used as a control. Quantitative data from 4 experiments are shown in bar graphs. (**B**) Strategy to generate mice with or without uterine ANP (uANP) and placental ANP (pANP). (**C**) Western blotting of uterine PRL and IGFBP1 in mice with or without uANP and pANP. Quantitative data from 4 experiments are shown in bar graphs. (**D**) Prolactin and IGFBP1 levels in the conditioned medium (CM) from HESCs cultured in non-differentiation (HESC) or decidualization (dHESC) medium with or without ANP. (**E**) Pro-ANP/ANP levels in the CM from cultured human villous trophoblasts (HVTs), human uterine SMCs (HUtSMCs), human uterine microvascular ECs (HUtMECs), HESCs, and dHESCs. (**F**) Prolactin levels in the CM from HESCs cultured in non-differentiation (HESC) or decidualization (dHESC) medium with or without HVT-derived CM. Quantitative data (mean ± SD) were analyzed by 1-way ANOVA (**A** and **D**–**F**) or Kruskal-Wallis test (**C**). In **D** and **F**, $^{*}P < 0.05$ and $^{**}P < 0.01$ for comparisons between HESC and dHESC or HESC+ANP and dHESC+ANP at the same time points; †$P < 0.05$ for comparisons between dHESC and dHESC+ANP at the same time points ($n = 3$ per group).

pro-ANP) was disrupted, and *Corin*$^{-/-}$ mice, in which ANP activation was abolished (25). In non-pregnant WT, *Nppa*$^{-/-}$, and *Corin*$^{-/-}$ mice, uterine prolactin and IGFBP1 protein levels were similar, as shown by Western blotting (Figure 1A). When the mice became pregnant after mating with males of the same genotype, uterine prolactin and IGFBP1 levels increased, as measured at gestational day (GD) 12.5 (Figure 1A). The levels, however, were lower in *Nppa*$^{-/-}$ and *Corin*$^{-/-}$ mice than in WT mice (Figure 1A). Consistently, mRNA levels of prolactin gene family members were also lower in pregnant *Nppa*$^{-/-}$ mouse uteri than in WT uteri (Supplemental Figure 1; supplemental material available online with this article; https://doi.org/10.1172/JCI151053DS1). These results indicate a role of the corin/ANP pathway in promoting uterine decidualization in mice.

ANP is expressed in the uterus and placenta (30, 36). To distinguish the role of uterine versus placental ANP in uterine decidualization, we mated *Nppa*$^{-/-}$ females with *Nppa*$^{+/-}$ males and *Nppa*$^{+/-}$ females with *Nppa*$^{-/-}$ males, resulting in *Nppa*$^{-/-}$ uteri with *Nppa*$^{+/-}$ or *Nppa*$^{-/-}$ placentas and *Nppa*$^{+/-}$ uteri with *Nppa*$^{+/-}$ or *Nppa*$^{-/-}$ placentas (Figure 1B). In Western blotting, uterine prolactin and IGFBP1 levels in *Nppa*$^{-/-}$ females with *Nppa*$^{+/-}$ placentas were higher than those in *Nppa*$^{-/-}$ females with *Nppa*$^{-/-}$ placentas, but lower than those in *Nppa*$^{+/-}$ females with *Nppa*$^{-/-}$ placentas (Figure 1C). These results indicate that while placental ANP is required for normal decidualization, uterine ANP is more important than placental ANP in this process.

ANP promotes decidualization in cultured HESCs. To verify the role of ANP in uterine decidualization, we cultured HESCs, a common model for studying decidualization in vitro (37). Upon induction to undergo differentiation, decidualized HESCs (dHESCs) expressed high levels of prolactin and IGFBP1 (Figure 1D). Addition of recombinant ANP to the differentiation medium further elevated prolactin and IGFBP1 levels, whereas such an effect was not observed if ANP was added to non-differentiation medium (Figure 1D). We next measured pro-ANP/ANP antigen in the conditioned medium (CM) from cultured human villous trophoblasts (HVTs), human uterine smooth muscle cells (HUtSMCs), human uterine microvascular endothelial cells (HUtMECs), HESCs, and

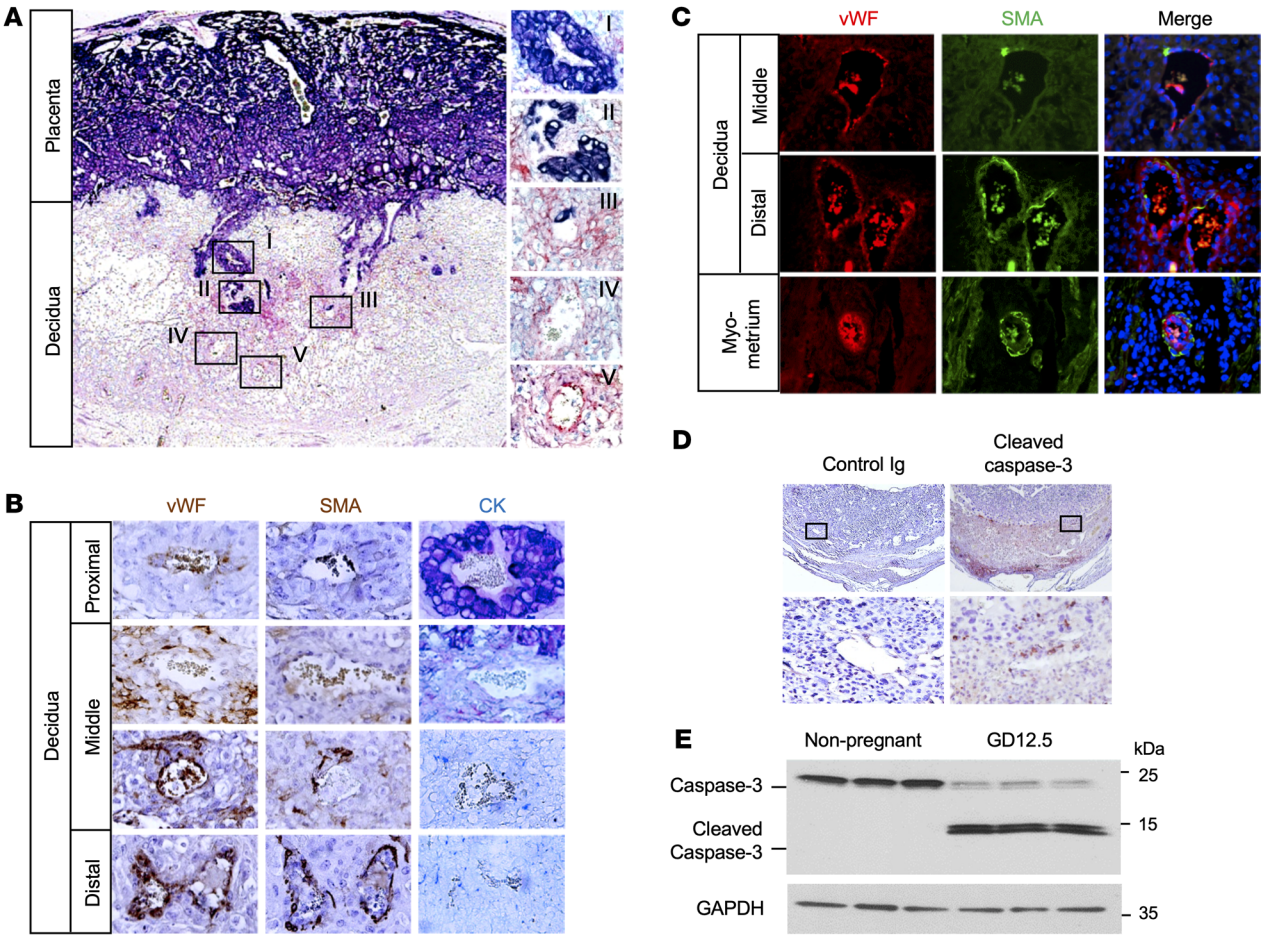

Figure 2. Uterine spiral artery remodeling and trophoblast invasion in pregnant mice. (**A**) Placental and decidual tissues from WT mice were collected at GD12.5. Longitudinal sections were stained for cytokeratin (CK) (blue) for trophoblasts and vWF (red) for ECs. Selected areas in the decidua are shown in a high original magnification (×400). Left panel shows lower original magnification (×100). (**B**) Transverse sections from proximal, middle, and distal decidual layers were stained for vWF (brown; left column) for ECs, SMA (brown; middle column) for SMCs, and CK (blue; right column) for trophoblasts. Images from a high original magnification (×400) are shown. (**C**) Coimmunofluorescent staining of transverse sections for vWF (red) and SMA (green) in middle (top row) and distal (middle row) decidual layers and the myometrium (bottom row). Images from a high original magnification (×400) are shown. (**D**) Staining of cleaved caspase-3 in uteroplacental sections from GD12.5-WT mice. Selected areas in the decidua are shown in a high original magnification (×400). Isotype-matched immunoglobulin (Ig) was used as a control. (**E**) Western blotting of caspase-3 fragments in uterine tissues from non-pregnant and GD12.5-WT mice (3 mice per group).

dHESCs. (The ELISA assay used in this experiment does not distinguish pro-ANP from ANP.) High levels of pro-ANP/ANP antigen were detected in the CM from HVTs, but not from HUtSMCs, HUtMECs, HESCs, and dHESCs (Figure 1E). When the CM from HVTs was added to the differentiation medium in HESCs, prolactin levels were increased, whereas such an effect was not observed if the HVT-derived CM was added to the non-differentiation medium in HESCs (Figure 1F). Together with the findings in *Nppa*$^{-/-}$ and *Corin*$^{-/-}$ mice, these results indicate that ANP promotes uterine decidualization and that in addition to uterine ANP, placental ANP also contributes to this process.

Sequential SMC and EC death in remodeling of spiral arteries. As reported previously (27), ANP deficiency impairs trophoblast invasion and uterine spiral artery remodeling in mice. To understand cellular dynamics during spiral artery remodeling, we stained GD12.5 uterine sections from WT mice with cytokeratin (for trophoblasts) and von Willebrand factor (vWF) (for ECs). Invading intravascular trophoblasts were observed in the proximal decidua (Figure 2A, panels I and II). In deeper decidual layers, where intravascular trophoblasts were barely detected (Figure 2A, panel III) or undetected (Figure 2A, panel IV), vWF-positive ECs were not detected on the lumen. Moreover, there were no detectable interstitial trophoblasts in surrounding tissues. In contrast, the endothelium was mostly intact in the distal decidua (Figure 2A, panel V). These results are consistent with previous reports (2, 38) indicating that during spiral artery remodeling, EC loss occurs before interstitial or intravascular trophoblast invasion.

To verify these results, we examined serial transverse uterine sections from WT mice at GD12.5. Spiral arteries in the proximal decidua had trophoblasts (cytokeratin) but not ECs (vWF) and SMCs (α-smooth muscle actin [SMA]) (Figure 2B, top row). (vWF is also present in plasma, and some vWF staining was found in residual blood clots in the artery and the tissue.) In sections from a middle decidual layer, where trophoblasts were

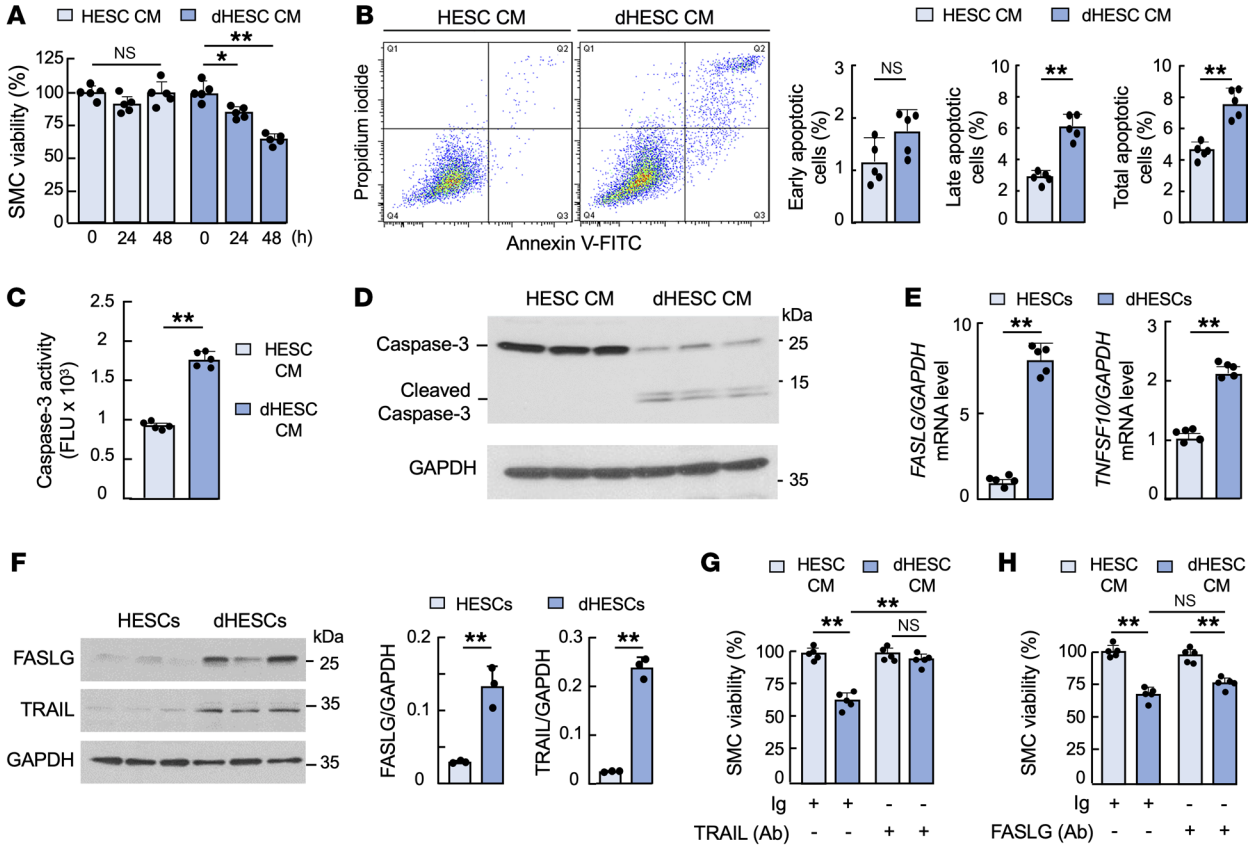

Figure 3. dHESC-mediated apoptosis in uterine SMCs. (**A**) Viability of HUtSMCs incubated with the CM from HESCs or dHESCs for different times (n = 5 per group). (**B**) Apoptosis in SMCs treated with HESC- or dHESC-derived CM for 48 hours was analyzed with flow cytometry. Percentages of early, late, and total apoptotic cells were measured (n = 5 per group). (**C**) Caspase-3 activity in SMCs treated with HESC- or dHESC-derived CM for 48 hours was examined with a fluorogenic assay. Data in relative fluorometric units (FLU) are presented (n = 5 per group). (**D**) Western blotting of caspase-3 fragments in SMCs treated with HESC- or dHESC-derived CM for 48 hours (n = 3 per group). (**E**) Quantitative real-time PCR analysis of *FASLG* and *TNFSF10* mRNA levels in HESCs and dHESCs (n = 5 per group). (**F**) Western blotting of FASLG and TRAIL in HESCs and dHESCs. Quantitative data are shown in bar graphs (n = 3 per group). (**G** and **H**) SMCs were incubated with CM from HESCs or dHESCs without (–) or with (+) immunodepletion of TRAIL (**G**) or FASLG (**H**) with an antibody (Ab) or control immunoglobulin (Ig). After 48 hours, cell viability was measured. All quantitative data are mean ± SD and were analyzed by 1-way ANOVA (**A**, **G**, and **H**) or Student's t test (**B**, **C**, **E**, and **F**). $^*P < 0.05$, $^{**}P < 0.01$.

about to enter the spiral artery, there was little vWF and SMA staining on the vessel wall (Figure 2B, second row). In sections from a deeper middle decidual layer, vWF staining was positive on most of the lumen, whereas little SMA and no cytokeratin staining was found in the vessel (Figure 2B, third row). In the distal decidua, vWF and SMA staining was on nearly the entire lumen and vessel wall, respectively, whereas cytokeratin was negative (Figure 2B, bottom row).

We also did costaining of vWF and SMA in similar transverse sections. In sections from the middle decidua, vWF staining was on most of the vessel lumen, whereas only residual SMA staining was in the vessel wall (Figure 2C, top row). In contrast, both vWF and SMA staining was on the entire vessel lumen and wall, respectively, in the distal decidua (Figure 2C, middle row) and the myometrium (Figure 2C, bottom row). The results from these complementary immunostaining experiments are consistent, indicating that during spiral artery remodeling, the loss of SMCs and ECs, probably due to apoptosis, occurs in a sequential manner before intravascular trophoblast invasion. Consistently, staining of cleaved caspase-3 (an apoptosis marker) was positive around spiral arteries in uterine sections from GD12.5-WT mice (Figure 2D). Western blotting also detected abundant cleaved caspase-3 fragments in GD12.5, but not non-pregnant, uterine tissues from WT mice (Figure 2E).

dHESCs secrete TRAIL to induce apoptosis in uterine SMCs. Decidual cells are active in secreting bioactive factors (39–41). To understand the mechanism underlying uterine SMC and EC death in the decidua, we tested the effect of dHESC-derived CM on uterine SMCs. Reduced viability (Figure 3A) and increased apoptosis (Figure 3B) were observed when HUtSMCs were incubated with the CM from dHESCs compared with that from non-differentiated HESCs. Increased caspase-3 activity (Figure 3C) and cleaved caspase-3 fragments (Figure 3D) were also found in HUtSMCs treated with dHESC-derived CM. These results support the idea that dHESCs may secret proapoptotic factor(s) to cause HUtSMC death.

We examined whether dHESCs express FAS ligand (FASLG), TNF-related apoptosis-inducing ligand (TRAIL), and TNF, which are major mediators in apoptosis. Compared with those in non-differentiated HESCs, *FASLG* and *TNFSF10* (encoding TRAIL) mRNA levels (Figure 3E) and FASLG and TRAIL protein

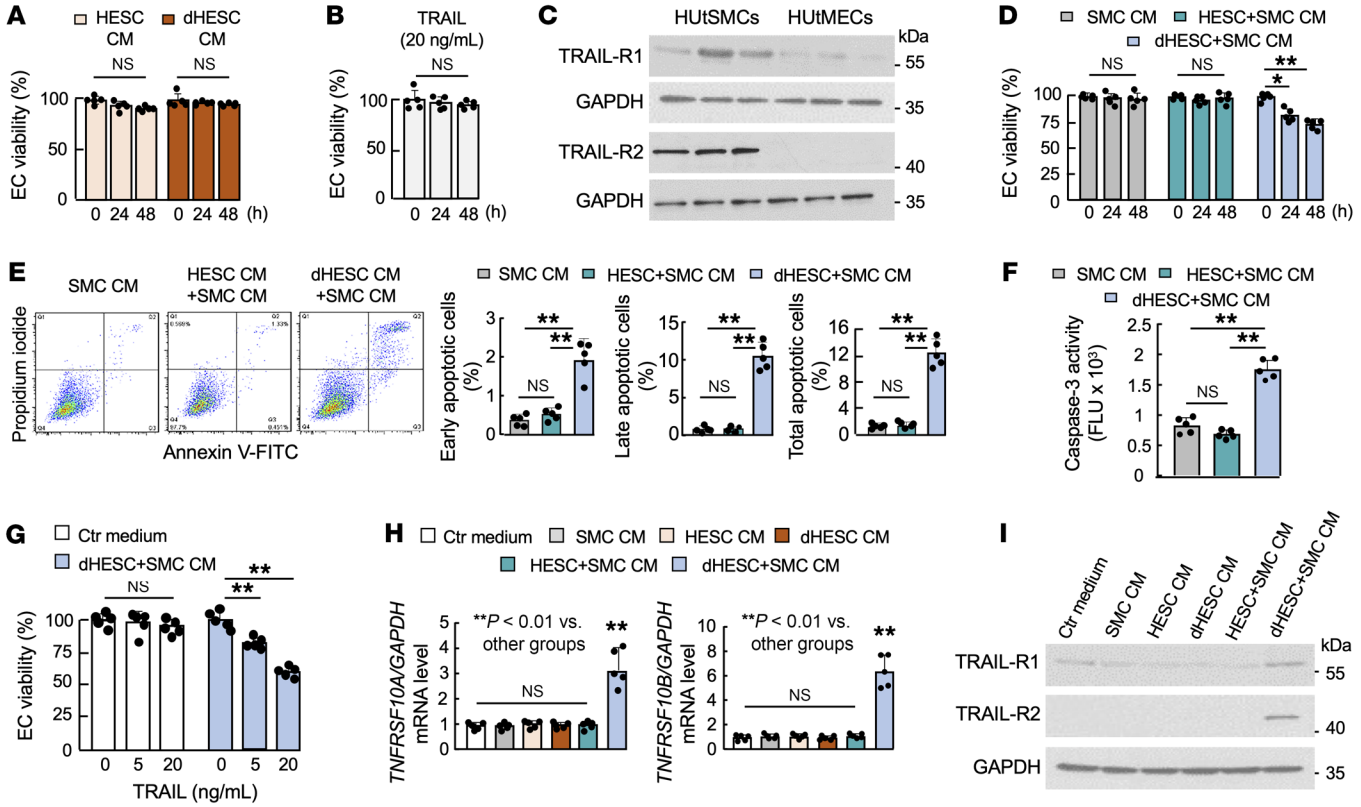

Figure 4. Apoptosis and TRAIL receptor upregulation in human uterine ECs. (**A** and **B**) Viability of HUtMECs treated with HESC- or dHESC-derived CM (**A**) or recombinant TRAIL (20 ng/mL) (**B**) over time (n = 5 per group). (**C**) Western blotting of TRAIL receptor (R) 1 and 2 in HUtSMCs and HUtMECs (n = 3 per group). (**D**–**F**) Viability (**D**), apoptosis (**E**), and caspase-3 activity (**F**) in HUtMECs incubated with CM from SMCs without (SMC CM) or with pretreatment of CM from HESCs (HESC+SMC CM) or dHESCs (dHESC+SMC CM). In **E** and **F**, incubation time was 48 hours. (**G**) TRAIL was added to HUtMECs treated with control (Ctr) medium or CM from SMCs pretreated with dHESC-derived CM. EC viability was measured (n = 5 per group). (**H** and **I**) *TNFRSF10A* and *TNFRSF10B* mRNA (**H**) and TRAIL receptor (R) 1 and 2 protein (**I**) levels were analyzed by real-time PCR and Western blotting, respectively, in HUtMECs treated with Ctr medium or CM from SMCs, HESCs, and dHESCs or SMCs pretreated with CM from HESCs or dHESCs. All quantitative data are mean ± SD and were analyzed by 1-way ANOVA (**A**, **B**, and **D**–**H**). *P < 0.05; **P < 0.01.

levels (Figure 3F) were increased in dHESCs, whereas *TNF* mRNA levels were not significantly changed (Supplemental Figure 2). To examine the potential role of FASLG and TRAIL in dHESC-mediated HUtSMC death, we used antibodies to deplete FASLG and TRAIL in dHESC-derived CM. Immunodepletion of TRAIL (Figure 3G), but not FASLG (Figure 3H), from dHESC-derived CM prevented HUtSMC death. Increased death was also observed when cultured HUtSMCs were treated with recombinant TRAIL (Supplemental Figure 3). These results indicate that TRAIL secreted from dHESCs is likely responsible for inducing apoptosis in uterine SMCs.

SMCs treated with dHESC-derived CM upregulate TRAIL receptor in ECs. We next tested whether dHESC-derived CM induces EC death. The viability of HUtMECs did not change significantly in the presence of CM from undifferentiated HESCs or dHESCs (Figure 4A) or recombinant TRAIL (Figure 4B). In real-time PCR (Supplemental Figure 4) and Western blotting (Figure 4C), *TNFRSF10A* and *TNFRSF10B* (encoding TRAIL receptors 1 and 2, respectively) mRNA levels and TRAIL receptor 1 and 2 protein levels were high in HUtSMCs but low or undetectable in HUtMECs, which may explain the apparent resistance of HUtMECs to TRAIL-induced death.

Unexpectedly, reduced viability (Figure 4D), increased apoptosis (Figure 4E), and high caspase-3 activity (Figure 4F) were found when HUtMECs were incubated with CM from SMCs that were pretreated with dHESC-derived CM, suggesting that dHESCs may induce EC death indirectly via an SMC-dependent mechanism. Indeed, HUtMECs became sensitive to TRAIL-induced death after incubation with CM from SMCs pretreated with dHESC-derived CM (Figure 4G). In real-time PCR (Figure 4H) and Western blotting (Figure 4I), upregulation of *TNFRSF10A* and *TNFRSF10B* mRNA levels and TRAIL receptor 1 and 2 protein levels was observed when HUtMECs were incubated with CM from SMCs that were pretreated with dHESC-derived CM. Such upregulation was not observed when HUtMECs were incubated with control medium or CM from SMCs, HESCs, dHESCs, or SMCs pretreated with HESC-derived CM (Figure 4, H and I). These results suggest that when exposed to dHESC-derived CM, SMCs may release factor(s) that upregulate TRAIL receptor in ECs, thereby subjecting ECs to TRAIL-induced death.

The MAPK/ERK pathway is involved in TRAIL receptor upregulation in ECs. The MAPK/ERK pathway activation has been reported to upregulate TRAIL receptor (42). We tested binimetinib, a MAPK/ERK signaling inhibitor (43), in our experiments.

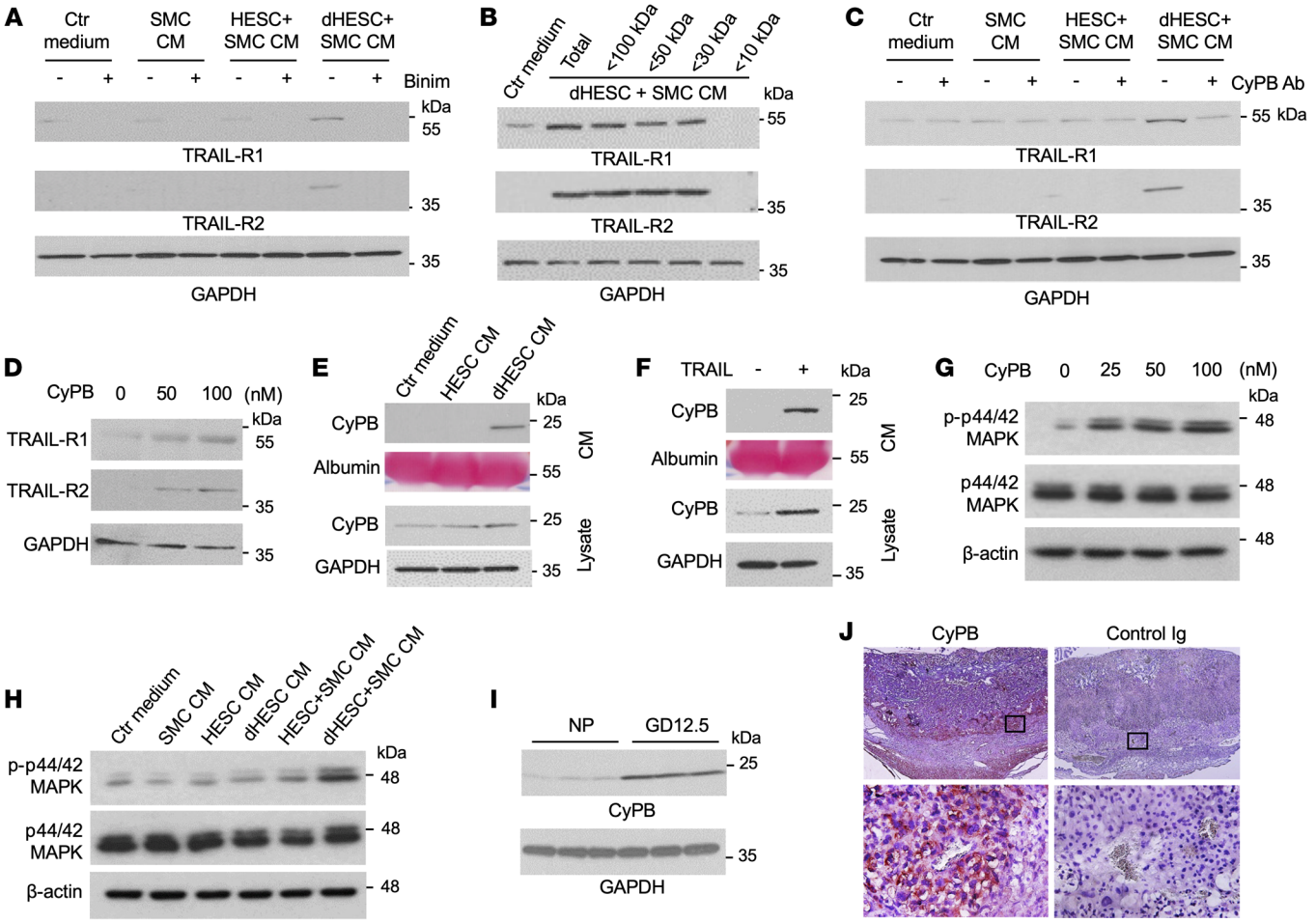

Figure 5. SMC-derived cyclophilin B upregulates TRAIL receptor in uterine ECs. (**A**) HUtMECs were incubated with control (Ctr) medium, or CM from SMCs without or with pretreatment of CM from HESCs or dHESCs in the presence (+) or absence (–) of binimetinib (Binim; 1 μM) for 48 hours. TRAIL-R1 and -R2 were analyzed by Western blotting. (**B**) Western blotting of TRAIL-R1 and -R2 in HUtMECs treated with unfractionated (Total) or fractionated CM with proteins of different molecular masses. (**C**) Cyclophilin B (CyPB) was depleted with an antibody (Ab) from SMC-derived CM. Western blotting was done for TRAIL-R1 and -R2 in HUtMECs treated with SMC-derived CM with (+) or without (–) CyPB depletion. (**D**) Western blotting of TRAIL-R1 and -R2 in HUtMECs treated with recombinant CyPB for 48 hours. (**E** and **F**) Uterine SMCs were treated with Ctr medium or CM from HESCs or dHESCs (**E**) or recombinant TRAIL (100 nM) (**F**) for 24 hours. Western blotting was done to examine CyPB in the CM (top) and cell lysates (bottom). Ponceau S–stained albumin in CM and GAPDH in lysates were controls. (**G** and **H**) Western blotting of phosphorylated (p) and total p44/42 MAPK in HUtMECs treated with recombinant CyPB (**G**) or different CM (**H**). (**I**) Western blotting of CyPB in non-pregnant (NP) and pregnant (GD12.5) uteri from WT mice. (**J**) CyPB staining in uterine sections from GD12.5-WT mice. Isotype-matched immunoglobulin (Ig) was a control (n = 3 per group). Selected areas of top panels (original magnification, ×40) are shown in lower panels (original magnification, ×400). Data are representative of at least 3 experiments.

In the presence of binimetinib, upregulation of TRAIL receptors 1 and 2 was blocked in HUtMECs that were incubated with CM from SMCs pretreated with dHESC-derived CM (Figure 5A). The results suggest that SMCs exposed to dHESC-derived CM may release MAPK/ERK–stimulating factor(s), which in turn upregulate TRAIL receptor in ECs.

To identify such factor(s), we fractionated, based on molecular masses, the CM from SMCs pretreated with dHESC-derived CM and tested the TRAIL receptor–upregulating activity in HUtMECs. We found that the activity was present in fractions with molecular masses less than 100, less than 50, and less than 30 kDa, but not in the fraction with molecular masses less than 10 kDa (Figure 5B). The results indicate that factor(s) with molecular mass(es) of 10–30 kDa in the CM from SMCs are responsible for upregulating TRAIL receptor in HUtMECs.

SMC-derived cyclophilin B upregulates TRAIL receptor in ECs. SMCs have been reported to release several factors under oxidative stress, and one of the factors is cyclophilin B, a 24 kDa protein that activates the MAPK/ERK pathway (44, 45). When we immunodepleted cyclophilin B in the CM from SMCs treated with dHESC-derived CM, the TRAIL receptor–upregulating activity was diminished (Figure 5C). When we treated HUtMECs with increasing concentrations of recombinant cyclophilin B, TRAIL receptor 1 and 2 protein levels were increased in a dose-dependent manner (Figure 5D). We also detected increased cyclophilin B expression and release in HUtSMCs treated with dHESC-derived CM (Figure 5E). Similarly, when HUtSMCs were treated with TRAIL, increased cyclophilin B expression and release were observed (Figure 5F). Moreover, when HUtMECs were treated with cyclophilin B (Figure 5G) or

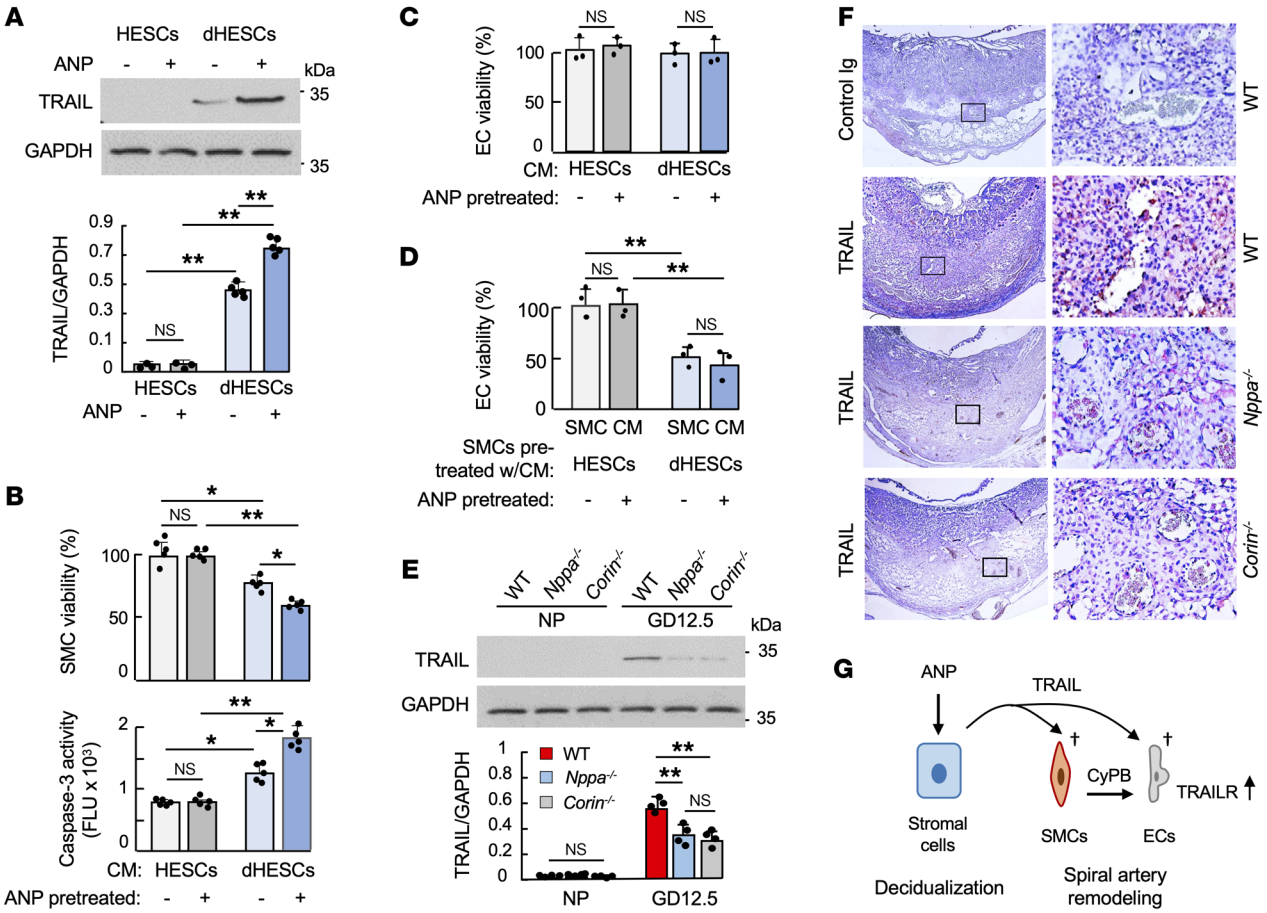

Figure 6. ANP upregulates TRAIL in dHESCs and uteri in pregnant mice. (**A**) Western blotting of TRAIL in HESCs and dHESCs cultured without (–) or with (+) recombinant ANP (1 nM). Quantitative data are shown in the bar graph (n = 5 per group). (**B**) Viability (top) and caspase-3 activity (bottom) in uterine SMCs treated with CM from HESCs or dHESCs without (–) or with (+) ANP pretreatment (n = 5 per group). (**C**) Viability of HUtMECs treated with CM from HESCs or dHESCs without (–) or with (+) ANP pretreatment (n = 3 per group). (**D**) Viability of HUtMECs treated with CM from SMCs that were incubated with CM from HESCs or dHESCs without (–) or with (+) ANP pretreatment (n = 3 per group). (**E**) Western blotting of uterine TRAIL in non-pregnant (NP) or pregnant (GD12.5) WT, *Nppa*$^{-/-}$, and *Corin*$^{-/-}$ mice. Quantitative data are shown in the bar graph (n = 4 per group). (**F**) TRAIL staining in GD12.5 uteri from WT, *Nppa*$^{-/-}$, and *Corin*$^{-/-}$ mice. Immunoglobulin (Ig) was a control. (**G**) A proposed model. ANP enhances decidualization and upregulates TRAIL in uterine stromal cells. TRAIL induces SMC death (†), leading to cyclophilin B (CyPB) release, which in turn upregulates TRAIL receptor (TRAILR) in ECs, causing EC death (†) in spiral arteries. All quantitative data are mean ± SD and were analyzed by 1-way ANOVA (**A**, **B**, **D**, and **E**) or Kruskal-Wallis test (**C**). $^*P < 0.05$; $^{**}P < 0.01$.

the CM from SMCs preincubated with dHESC-derived CM (Figure 5H), increased phosphorylation of p44/42 MAPK (ERK1/2) was detected by Western blotting. Western blotting also detected high cyclophilin B levels in GD12.5 uteri compared with those in non-pregnant uteri in WT mice (Figure 5I). In immunohistochemistry, strong cyclophilin B staining was detected around spiral arteries in GD12.5 uterine sections (Figure 5J). These results suggest that cyclophilin B released from apoptotic SMCs may play an important role in TRAIL receptor upregulation and subsequent TRAIL-mediated apoptosis in ECs.

ANP enhances TRAIL expression in dHESCs and dHESC-mediated SMC death. Given the role of ANP in uterine decidualization and the role of dHESC-derived TRAIL in SMC death indicated in our experiments, we next examined the effect of ANP on TRAIL expression in dHESCs and dHESC-mediated SMC death. When ANP was added to differentiation, but not non-differentiation, medium, TRAIL protein levels were increased in dHESCs (Figure 6A). Consistently, decreased viability, higher caspase-3 activity (Figure 6B), and increased apoptosis (Supplemental Figure 5) were observed when HUtSMCs were incubated with CM from dHESCs that were pretreated with ANP, compared with CM from dHESCs without ANP pretreatment or from non-differentiated HESCs with or without ANP pretreatment. We did not observe significant changes in viability when HUtMECs were cultured with CM from HESCs or dHESCs with or without ANP pretreatment (Figure 6C). In contrast, decreased viability was observed when HUtMECs were exposed to CM from SMCs that were pretreated with CM from dHESCs with or without ANP pretreatment (Figure 6D). These results indicate an important role of ANP in upregulating TRAIL in decidualized endometrial cells, which induces apoptosis in SMCs and, indirectly, in ECs.

Uterine TRAIL level is reduced in pregnant Nppa$^{-/-}$ *mice.* To verify our findings, we examined uterine TRAIL levels in mice. By Western blotting, we found that uterine TRAIL levels were undetectable in non-pregnant WT, *Nppa*$^{-/-}$, and *Corin*$^{-/-}$ mice, but the

levels were increased in all 3 strains of mice at GD12.5 (Figure 6E). Compared with that in pregnant WT mice, uterine TRAIL levels in pregnant *Nppa*$^{-/-}$ and *Corin*$^{-/-}$ mice were much lower (Figure 6E). In immunohistochemistry, TRAIL staining was stronger in uterine sections from GD12.5-WT mice, compared with that from GD12.5-*Nppa*$^{-/-}$ and *Corin*$^{-/-}$ mice (Figure 6F and Supplemental Figure 6), which is consistent with the findings in cultured dHESCs (Figure 6A). Together, our results indicate an important ANP function in promoting uterine decidualization and upregulating TRAIL in decidualized stromal cells, which leads to vascular SMC death and cyclophilin B release. SMC-derived cyclophilin B in turn upregulates TRAIL receptor in ECs, thereby causing TRAIL-mediated EC death in spiral arteries (Figure 6G).

Pro-ANP processing and gene expression in HVTs and placentas. In cultured human villous trophoblast (HVTs), we showed that WT corin converted pro-ANP to ANP whereas the corin mutant S472G, identified in preeclamptic women (27), had no detectable pro-ANP processing activity (Supplemental Figure 7). By quantitative real-time PCR, we found reduced *TNFSF10* and *CORIN* mRNA levels in preeclamptic placentas compared with those in normal controls. In contrast, *NPPA* and *PPIB* (encoding cyclophilin B) mRNA levels were higher in preeclamptic placentas, whereas *TNFRSF10A* and *TNFRSF10B* mRNA levels were similar between preeclamptic and normal placentas (Supplemental Figure 8). These results suggest that there may be alterations of corin/ANP and TRAIL pathways in preeclamptic placentas and that the ANP- and TRAIL-mediated mechanism may be more important in the uterus than in the placenta in regulating spiral artery remodeling.

Discussion

In pregnancy, uterine corin and ANP promote trophoblast invasion and spiral artery remodeling (27, 46), but the underlying mechanism remains unclear. In this study, we identified an important ANP function in enhancing uterine decidualization. By analyzing mice lacking either uterine or placental ANP, we found that both uterine and placental ANP is required for decidualization, but that lacking uterine ANP had a greater detrimental effect on decidualization. These results are consistent with previous findings that uterine corin is more important than placental corin in promoting trophoblast invasion and spiral artery remodeling in mice (27).

Decidualization is essential for embryo implantation, trophoblast invasion, and spiral artery remodeling (9, 35). Both endometrial stromal cells and invading trophoblasts are known to secrete proapoptotic factors, including FASLG, TNF, and TRAIL (47–51). It has been shown that trophoblast-derived FASLG, TNF, and TRAIL induce arterial SMC and EC apoptosis in vitro and in in vivo models (52–54). In immunostaining to examine cell dynamics during spiral artery remodeling, we found that the loss of SMA and vWF staining, which may reflect the loss of vascular SMCs and ECs, respectively, occurred in a sequential manner. Importantly, the cell loss was detected in vascular segments where no interstitial or intervascular trophoblast invasion was observed. These results indicate that the initial cell death in spiral arteries is likely mediated by factors from decidual stromal cells, but not trophoblasts. Undoubtedly, subsequent invading trophoblasts could further enhance uterine tissue and vascular remodeling.

TRAIL-dependent apoptosis is an important mechanism in eliminating poorly decidualized stromal cells in the pregnant uterus (55). In our study, incubation with the CM from dHESCs, but not non-differentiated HESCs, caused apoptosis in uterine SMCs. The apoptosis was prevented when TRAIL, but not FASLG, was immunodepleted from the dHESC-derived CM. Consistent with findings in previous gene analysis (56), we showed that *TNFSF10* mRNA and TRAIL protein levels were increased in dHESCs. These results indicate that TRAIL from decidualized endometrial stromal cells is likely a key factor that causes SMC death in spiral arteries.

Unlike vascular SMCs, ECs are resistant to FAS-mediated apoptosis (57). Consistently, no apparent apoptosis occurred when HUtMECs were incubated with dHESC-derived CM or recombinant TRAIL. The resistance to TRAIL-mediated apoptosis is likely due to low levels of TRAIL receptor on HUtMECs, as indicated in our study. Previously, TRAIL receptor was detected in different stromal cell populations in uterine tissues from pregnant women (56). It appears that selective TRAIL receptor expression is a key mechanism in regulating apoptosis in the pregnant uterus.

The observation of the sequential loss of SMCs and ECs suggests that apoptotic SMCs may be part of the mechanism in EC death. Indeed, treatment of CM from SMCs preincubated with dHESC-derived CM increased TRAIL receptor levels and caused apoptosis in HUtMECs. Previously, MAPK/ERK signaling was shown to increase TRAIL receptor 1 (also called death receptor 4) levels in cancer cells (42). TRAIL-induced apoptosis is known to be associated with reactive oxygen species (ROS) generation (58, 59). It has been reported that upon ROS stimulation, vascular SMCs release factors, such as heat shock protein 90-α and cyclophilin B, that activate the MAPK/ERK pathway (45). Similarly, cyclophilin B binding to its cell surface receptor, CD147, enhances MAPK/ERK signaling in human hepatic cancer cells (44).

In our study, the SMC-derived TRAIL receptor–upregulating activity was found in a fraction with proteins of approximately 10–30 kDa. In experiments with binimetinib, cyclophilin B immunodepletion, and recombinant cyclophilin B treatment, we identified cyclophilin B as a likely factor from SMCs that upregulated TRAIL receptor in uterine vascular ECs. We also showed that ANP treatment increased TRAIL levels in dHESCs and that in TRAIL-treated HUtSMCs, cyclophilin B expression and release were increased. Moreover, low uterine TRAIL levels were found in pregnant *Nppa*$^{-/-}$ and *Corin*$^{-/-}$ mice. Together, these results suggest that ANP promotes decidualization and TRAIL expression in endometrial stromal cells, thereby causing SMC death and cyclophilin B release in spiral arteries. Cyclophilin B in turn enhances ERK signaling and TRAIL receptor expression in ECs, leading to TRAIL-induced apoptosis. This mechanism could explain the observed sequential SMC and EC death in remodeling of uterine spiral arteries.

Impaired spiral artery remodeling, including incomplete loss of SMCs and ECs, is a major pathological feature in preeclampsia, a disease known to be associated with endothelial dysfunction (60). Our findings of a potential role of ANP in decidualization and TRAIL-mediated SMC and EC death should encourage more studies to verify the role of uterine TRAIL and related molecules in spiral artery remodeling in other animal models and to examine whether

defects in ANP and TRAIL pathways contribute to preeclampsia in humans. It is worth pointing out that decidualization occurs in the late secretory phase of the human menstrual cycle, which does not happen in mice. Further studies will be important to examine whether TRAIL-dependent EC loss occurs during the menstrual cycle in humans. Findings from such studies may provide new mechanistic insights into menstruation-associated disorders.

In summary, uterine decidualization, trophoblast invasion, and spiral artery remodeling are important processes in pregnancy (9, 35, 61). Defects in these processes are major contributing factors in preeclampsia (4, 6–8, 14). In this study, we uncover a novel ANP function in promoting uterine decidualization and a TRAIL-mediated mechanism to eliminate SMCs and ECs in spiral arteries. These uterine cellular changes are expected to facilitate trophoblast invasion, both interstitially and intravascularly. Invading trophoblasts could provide additional factors, including ANP, to enhance decidualization and spiral artery remodeling. Thus, our results highlight a key role of ANP in a reciprocal mechanism that regulates the interplay among multiple cell types at the uteroplacental interface.

Methods

Cell culture. Human uterine smooth muscle cells (HUtSMCs) (PromoCell, C-12576) were cultured in SMC growth medium (PromoCell, C-22062) with 1% penicillin. Human uterine microvascular endothelial cells (HUtMECs) (PromoCell, C-12296) were cultured in EC growth medium (PromoCell, C-22020). Human villous trophoblasts (HVTs) (ScienCell, 7120) were cultured in trophoblast medium (ScienCell, 7121). HESCs, a transformed cell line (ATCC, CRL-4003), were cultured in DMEM and Ham's F-12 medium (Sigma-Aldrich, D2906) (1:1) with 10% charcoal-dextran–stripped FBS (Life Technologies, A3382101), 3.1 g/L glucose, 1 mM sodium pyruvate, 1.2 g/L sodium bicarbonate, 1% ITS (insulin, human transferrin, and selenous acid) with premix universal culture supplement (Thermo Fisher Scientific, CB40352), and 500 ng/mL puromycin (Thermo Fisher Scientific, ICN19453925). All the cells were cultured at 37°C in humidified incubators with 5% CO_2.

Induction of decidualization in HESCs. Cultured HESCs (~90% confluence) were induced to undergo decidualization in DMEM/F-12 medium with 1 μM medroxyprogesterone acetate (Acros Organics, AC461120010), 10 nM estradiol (Sigma-Aldrich, E2758), and 0.2 mM 8-bromo-cAMP (Thermo Fisher Scientific, AAJ64469MF). HESCs with the regular DMEM/F-12 medium, described above, were used as undifferentiated controls. To examine the effect of ANP on HESCs, recombinant ANP (10 nM; MilliporeSigma, 0523030005M) was added to differentiation and non-differentiation medium. At different time points, the CM was collected and measured for prolactin and IGFBP1 with ELISA (Thermo Fisher Scientific, DPRL00 and DY871-05). To examine the effect of HESC-derived medium on SMCs and ECs, human uterine SMCs and ECs were cultured in 96- or 6-well plates for 24 hours. After washing with PBS, CM, which was incubated with HESCs or dHESCs for 24 hours, was added to SMCs or ECs (0.1 mL/well and 1 mL/well for 96- and 6-well plates, respectively). After 24 or 48 hours at 37°C, cell viability, apoptosis, caspase-3 activity, and gene/protein expression were examined, as described below. In a subset of experiments, CM from SMCs pretreated with dHESC- or HESC-derived CM for 24 hours was incubated with ECs to examine the effect on cell death and gene/protein expression.

Cell viability. Cell viability was measured in HUtSMCs and HUtMECs that were incubated with CM from HESCs or dHESCs or recombinant TRAIL (BioLegend, 752904) over time. After washing, a solution from the CellTiter-Blue Cell Viability Assay kit (Promega, G8080) was added. Cell viability was analyzed, according to the manufacturer's instructions.

Apoptosis detection. Cells were detached with trypsin-EDTA (VWR, 45000-658) treatment, centrifuged at 110*g* for 8 minutes, and washed twice with ice-cold PBS. The cells were resuspended in binding buffer (BioLegend, 640914), added to a solution with annexin V–FITC and propidium iodide (BioLegend, 421301), and subjected to analysis by flow cytometry (Becton Dickinson LSR II). The data were analyzed by FlowJo software (BD Biosciences).

Caspase-3 activity assay. Cells were cultured in 96-well plates. Apo-ONE caspase-3 reagent (100 μL; Promega, G7792) was added to each well. Wells without cells were included as controls. The plates were placed on a shaker for 30 seconds and incubated at room temperature for 4 hours. Fluorescent signals in the wells were measured with a plate reader (Becton Dickinson LSR II) with excitation (499 nm) and emission (521 nm) wavelengths. The data were analyzed by FlowJo software.

Western blotting. Cell lysates were prepared with lysis buffer containing 50 mM Tris-HCl (pH 7.4), 150 mM NaCl, 1% (vol/vol) NP-40, 1% sodium deoxycholate, 0.1% SDS, and 2% (vol/vol) protease inhibitor cocktail (Thermo Fisher Scientific, 78442). To analyze uterine proteins in pregnant mice, tissues underlying the individual implantation sites were dissected out, added to tubes containing the lysis buffer (0.5 mL buffer/100 mg tissue) and three 5-mm stainless steel beads (Qiagen, 69989), homogenized with TissueLyser II (25 Hz, 1 minute; Qiagen), and centrifuged (15,000*g*, 10 minutes) at 4°C. The supernatant was transferred to a new tube. Proteins in CM, cell lysates, and tissue homogenates were separated by 4%–20% gradient SDS-PAGE and transferred onto PVDF (Bio-Rad, 1620177) membranes. The primary and secondary antibodies used in Western blotting are listed in Supplemental Table 1. As a protein loading control, GAPDH was verified with an antibody (MilliporeSigma, MAB3740). After the ECL Western blotting substrate (Thermo Fisher Scientific, 32109) was applied, the membranes were exposed to x-ray films. The intensity of protein bands was quantified using Gel-Pro Analyzer 4.0 software (Media Cybernetics).

Real-time PCR and quantitative real-time PCR. Total RNAs were isolated from tissues and cells using TRIzol reagent (Invitrogen, 15596018), PureLink RNA kit (Invitrogen, 12183018A), or DirectZol mRNA kit (Zymo Research, R2052). RNA purity and concentration were determined using a spectrometer (Thermo Fisher Scientific, Nanodrop 2000c). mRNAs were used to make cDNAs using iScript cDNA Synthesis kit (Bio-Rad, 1708891) for real-time PCR and quantitative real-time PCR. Quantitative real-time PCR was done using QuantStudio 5 (Thermo Fisher Scientific, A28574) with SYBR Green Master Mix (Bio-Rad, 1708882; Midwest Scientific, BEQPCR-S or BEQPCRLR). The gene-specific primers used are listed in Supplemental Table 2.

Mice. *Corin*$^{-/-}$ mice were generated and characterized as reported previously (25, 62). *Nppa*$^{-/-}$ mice (B6.129P2-*Nppa*^{tm1Unc}/J), originally from The Jackson Laboratory, were described in our previous studies (27). *Nppa*$^{+/-}$ mice were generated by mating of *Nppa*$^{-/-}$ and C57BL/6J WT mice. Female mice (3–4 months old) were mated and checked for vaginal plugs to establish gestation timing. The day when a plug was

observed was defined as GD0.5. At different times, mice were euthanized by CO_2 inhalation followed by cervical dislocation. Tissues were isolated for further experiments.

Histology and immune staining. Mouse uterine and placental tissues were fixed in 4% paraformaldehyde, dehydrated in ethanol, and embedded in paraffin. Sections were cut (10 μm in thickness). Immunohistochemistry was done with antibodies against SMA (1:200; Cell Signaling Technology, 19245T) (Supplemental Table 1), vWF (1:100; Thermo Fisher Scientific, PA5-16634), pan-cytokeratin (1:100; Cell Signaling Technology, 4545S), cleaved caspase-3 (1:200; Cell Signaling Technology, 9661T), TRAIL (1:150; R&D Systems, AF1121), and cyclophilin B (1:200; Thermo Fisher Scientific, MAB5410-SP). Isotype-matched immunoglobulin was used as a control. Secondary antibodies included HRP- or alkaline phosphatase–conjugated anti-rabbit (Cell Signaling Technology, 8114p) and anti-mouse (Thermo Fisher Scientific, 31320) antibodies that were detected with substrate kits (Vector Laboratories, SK-4800 and SK-5400). Stained sections were examined under a light microscope (Olympus BX51). In studies with mouse embryos, tissue samples from at least 3–4 mice per group and at least 2 implant sites per mouse were used. In serial sections, the position of the maternal artery and the depth of the trophoblast invasion site were used as a guide. At least 4–6 sections from the center of the placenta of each embryo were used for immunohistochemical analysis. To quantify staining intensity, images were analyzed by ImageJ software (NIH).

Protein fractionation. The CM was collected from uterine SMCs that were pretreated with dHESC-derived CM. Fifteen milliliters of CM was added to each Amicon Ultra filter device (MilliporeSigma) with different molecular weight cutoff values (100 kDa, UFC910024; 50 kDa, UFC905024; 30 kDa, UFC903024; and 10 kDa, UFC901024). The devices were centrifuged at 4000*g* for 20 minutes. The fractioned CM was collected and tested on HUtMECs for TRAIL receptor–upregulating activity.

Cyclophilin B analysis. Human recombinant cyclophilin B (25–100 nM; Sigma-Aldrich, SRP6066) or control vehicle was incubated with HUtMECs at 37°C for 48 hours. Cell lysates were prepared for Western blotting of TRAIL receptor. In another set of experiments, HUtMECs were incubated with cyclophilin B or different types of CM at 37°C for 30 minutes. Cell lysates were prepared for p44/42 MAPK (ERK1/2) phosphorylation analysis by Western blotting. For cyclophilin B expression and release from HUtSMCs, the cells were treated with recombinant human TRAIL (100 nM; BioLegend, 752904) or CM from HESCs or dHESCs for 48 hours. The CM and cell lysates were prepared as described above. Cyclophilin B in the CM and cell lysates was examined by immunoprecipitation and Western blotting (63) with an anti–cyclophilin B antibody (1 μg/mL; Thermo Fisher Scientific, MAB5410SP).

Pro-ANP processing in HVTs. HVTs were cultured in 6-well plates, as described above. Plasmids expressing human pro-ANP and corin WT or mutants including S472G, identified in preeclamptic women (27), and R801A, lacking the catalytic activity (33), were transfected into the cells using PolyJet mixtures (SignaGen Laboratories, SL100688). Both recombinant pro-ANP and corin contained a C-terminal V5 tag. After 24 hours at 37°C, the CM was collected and cell lysates were prepared, as described above. Pro-ANP and ANP fragments in the CM and corin protein in lysates were examined by Western blotting using an HRP-conjugated anti-V5 antibody (Thermo Fisher Scientific, R96125), as described previously (33).

Human placental tissues. Human placental samples from women with normal pregnancy (n = 10) and with preeclampsia (n = 11) were collected and stored at –80°C at the Suzhou Municipal Hospital affiliated with Nanjing Medical University in China. Participant characteristics are listed in Supplemental Table 3. Placental gene expression was analyzed by quantitative real-time PCR, as described above.

Statistics. Analyses were conducted using Prism 9 software (GraphPad Software). The normality of data distribution was analyzed by the Anderson-Darling test. Comparisons were made by 2-tailed Student's t test (between 2 groups) and ANOVA and Tukey's post hoc analysis (among multiple groups) or nonparametric Mann-Whitney test (between 2 groups) and Kruskal-Wallis test (among multiple groups). Results are presented as mean ± SD. Fisher's exact test was used to compare categorical data. A P value less than 0.05 was considered significant.

Study approval. The study in mice was approved by the Cleveland Clinic Institutional Animal Care and Use Committee (2018-1964). All procedures were conducted according to the approved protocol and in accordance with the NIH guidelines for the ethical treatment and handling of animals in research. The study involving human tissues was approved by the ethics committee of the Suzhou Municipal Hospital (2019-118) and conducted in accordance with the Declaration of Helsinki. All participants provided written informed consent.

Author contributions

QW conceived and supervised the project. WZ, SL, JL, HL, ML, and ND designed and performed the experiments and collected the data. WZ, SL, JL, HL, ML, ND, and QW analyzed and discussed the data. WZ and QW wrote the first draft of the manuscript. All authors critically read and commented on the manuscript and approved the final version for submission.

Acknowledgments

This work was supported in part by grants from the NIH (HD093727 to QW), the American Heart Association (19POST34380460 to SL), and the National Natural Science Foundation of China (81901499 to HL and 81873840 to ND).

Address correspondence to: Qingyu Wu, Cyrus Tang Hematology Center, Soochow University, 199 Ren Ai Road, Suzhou 215123, China. Phone: 86.512.65880877; Email: qywu88@yahoo.com.

1. Norwitz ER, et al. Implantation and the survival of early pregnancy. *N Engl J Med*. 2001;345(19):1400–1408.
2. Whitley GS, Cartwright JE. Cellular and molecular regulation of spiral artery remodelling: lessons from the cardiovascular field. *Placenta*. 2010;31(6):465–474.
3. Burton GJ, et al. Rheological and physiological consequences of conversion of the maternal spiral arteries for uteroplacental blood flow during human pregnancy. *Placenta*. 2009;30(6):473–482.
4. Chaiworapongsa T, et al. Pre-eclampsia part 1: current understanding of its pathophysiology. *Nat Rev Nephrol*. 2014;10(8):466–480.
5. Steegers EA, et al. Pre-eclampsia. *Lancet*. 2010;376(9741):631–644.
6. Pijnenborg R, et al. The uterine spiral arteries in human pregnancy: facts and controversies. *Placenta*. 2006;27(9-10):939–958.
7. Fisher SJ. Why is placentation abnormal in preeclampsia? *Am J Obstet Gynecol*.

2015;213(4 suppl):S115–S122.
8. Redman CW, Sargent IL. Latest advances in understanding preeclampsia. *Science*. 2005;308(5728):1592–1594.
9. Mori M, et al. The decidua—the maternal bed embracing the embryo—maintains the pregnancy. *Semin Immunopathol*. 2016;38(6):635–649.
10. Brosens JJ, et al. The myometrial junctional zone spiral arteries in normal and abnormal pregnancies: a review of the literature. *Am J Obstet Gynecol*. 2002;187(5):1416–1423.
11. Craven CM, et al. Decidual spiral artery remodelling begins before cellular interaction with cytotrophoblasts. *Placenta*. 1998;19(4):241–252.
12. Kam EP, et al. The role of trophoblast in the physiological change in decidual spiral arteries. *Hum Reprod*. 1999;14(8):2131–2138.
13. Avagliano L, et al. Abnormal spiral artery remodelling in the decidual segment during pregnancy: from histology to clinical correlation. *J Clin Pathol*. 2011;64(12):1064–1068.
14. Conrad KP, et al. Emerging role for dysregulated decidualization in the genesis of preeclampsia. *Placenta*. 2017;60:119–129.
15. Garrido-Gomez T, et al. Defective decidualization during and after severe preeclampsia reveals a possible maternal contribution to the etiology. *Proc Natl Acad Sci U S A*. 2017;114(40):E8468–E8477.
16. Rabaglino MB, et al. Bioinformatics approach reveals evidence for impaired endometrial maturation before and during early pregnancy in women who developed preeclampsia. *Hypertension*. 2015;65(2):421–429.
17. Song W, et al. Atrial natriuretic peptide in cardiovascular biology and disease (NPPA). *Gene*. 2015;569(1):1–6.
18. Kuhn M. Molecular physiology of membrane guanylyl cyclase receptors. *Physiol Rev*. 2016;96(2):751–804.
19. Cannone V, et al. Atrial natriuretic peptide: a molecular target of novel therapeutic approaches to cardio-metabolic disease. *Int J Mol Sci*. 2019;20(13):3265.
20. Goetze JP, et al. Cardiac natriuretic peptides. *Nat Rev Cardiol*. 2020;17(11):698–717.
21. Špiranec Spes K, et al. Natriuretic peptides attenuate retinal pathological neovascularization via cyclic guanosine monophosphate signaling in pericytes and astrocytes. *Arterioscler Thromb Vasc Biol*. 2020;40(1):159–174.
22. Yan W, et al. Corin, a transmembrane cardiac serine protease, acts as a pro-atrial natriuretic peptide-converting enzyme. *Proc Natl Acad Sci U S A*. 2000;97(15):8525–8529.
23. Dong N, et al. Function and regulation of corin in physiology and disease. *Biochem Soc Trans*. 2020;48(5):1905–1916.
24. Yan W, et al. Corin, a mosaic transmembrane serine protease encoded by a novel cDNA from human heart. *J Biol Chem*. 1999;274(21):14926–14935.
25. Chan JC, et al. Hypertension in mice lacking the proatrial natriuretic peptide convertase corin. *Proc Natl Acad Sci U S A*. 2005;102(3):785–790.
26. Chen S, et al. PCSK6-mediated corin activation is essential for normal blood pressure. *Nat Med*. 2015;21(9):1048–1053.
27. Cui Y, et al. Role of corin in trophoblast invasion and uterine spiral artery remodelling in pregnancy. *Nature*. 2012;484(7393):246–250.
28. Wang C, et al. Krüppel-like factor 17 upregulates uterine corin expression and promotes spiral artery remodeling in pregnancy. *Proc Natl Acad Sci U S A*. 2020;117(32):19425–19434.
29. Kaitu'u-Lino TJ, et al. Corin, an enzyme with a putative role in spiral artery remodeling, is up-regulated in late secretory endometrium and first trimester decidua. *Hum Reprod*. 2013;28(5):1172–1180.
30. Reis AM, et al. Regulation of the natriuretic peptide system in rat uterus during the estrous cycle. *J Endocrinol*. 1997;153(3):345–355.
31. Badrov MB, et al. Role of corin in blood pressure regulation in normotensive and hypertensive pregnancy. *Hypertension*. 2019;73(2):432–439.
32. Armstrong DW, et al. Gestational hypertension in atrial natriuretic peptide knockout mice and the developmental origins of salt-sensitivity and cardiac hypertrophy. *Regul Pept*. 2013;186:108–115.
33. Dong N, et al. Corin mutations K317E and S472G from preeclamptic patients alter zymogen activation and cell surface targeting [corrected]. *J Biol Chem*. 2014;289(25):17909–17916.
34. Stepanian A, et al. Highly significant association between two common single nucleotide polymorphisms in CORIN gene and preeclampsia in Caucasian women. *PLoS One*. 2014;9(12):e113176.
35. Gellersen B, et al. Decidualization of the human endometrium: mechanisms, functions, and clinical perspectives. *Semin Reprod Med*. 2007;25(6):445–453.
36. Graham CH, et al. Expression of atrial natriuretic peptide by third-trimester placental cytotrophoblasts in women. *Biol Reprod*. 1996;54(4):834–840.
37. Zhu H, et al. Endometrial stromal cells and decidualized stromal cells: origins, transformation and functions. *Gene*. 2014;551(1):1–14.
38. Pijnenborg R, et al. Uteroplacental arterial changes related to interstitial trophoblast migration in early human pregnancy. *Placenta*. 1983;4(4):397–413.
39. Sharma S, et al. Decidual control of trophoblast invasion. *Am J Reprod Immunol*. 2016;75(3):341–350.
40. Hess AP, et al. Decidual stromal cell response to paracrine signals from the trophoblast: amplification of immune and angiogenic modulators. *Biol Reprod*. 2007;76(1):102–117.
41. Lash GE, Ernerudh J. Decidual cytokines and pregnancy complications: focus on spontaneous miscarriage. *J Reprod Immunol*. 2015;108:83–89.
42. Yao W, et al. Expression of death receptor 4 is positively regulated by MEK/ERK/AP-1 signaling and suppressed upon MEK inhibition. *J Biol Chem*. 2016;291(41):21694–21702.
43. Tran B, Cohen MS. The discovery and development of binimetinib for the treatment of melanoma. *Expert Opin Drug Discov*. 2020;15(7):745–754.
44. Kim K, et al. Release of overexpressed CypB activates ERK signaling through CD147 binding for hepatoma cell resistance to oxidative stress. *Apoptosis*. 2012;17(8):784–796.
45. Liao DF, et al. Purification and identification of secreted oxidative stress-induced factors from vascular smooth muscle cells. *J Biol Chem*. 2000;275(1):189–196.
46. Zhou Y, Wu Q. Role of corin and atrial natriuretic peptide in preeclampsia. *Placenta*. 2013;34(2):89–94.
47. Whitley GS, Cartwright JE. Trophoblast-mediated spiral artery remodelling: a role for apoptosis. *J Anat*. 2009;215(1):21–26.
48. Bulmer JN, et al. The role of vascular smooth muscle cell apoptosis and migration during uterine spiral artery remodeling in normal human pregnancy. *FASEB J*. 2012;26(7):2975–2985.
49. Kayisli UA, et al. Human chorionic gonadotropin contributes to maternal immunotolerance and endometrial apoptosis by regulating Fas-Fas ligand system. *J Immunol*. 2003;171(5):2305–2313.
50. Gu Y, et al. Apoptosis in decidual tissue regression and reorganization. *Endocrinology*. 1994;135(3):1272–1279.
51. Chan J, et al. Glucocorticoid-induced apoptosis in human decidua: a novel role for 11beta-hydroxysteroid dehydrogenase in late gestation. *J Endocrinol*. 2007;195(1):7–15.
52. Keogh RJ, et al. Fetal-derived trophoblast use the apoptotic cytokine tumor necrosis factor-alpha-related apoptosis-inducing ligand to induce smooth muscle cell death. *Circ Res*. 2007;100(6):834–841.
53. Ashton SV, et al. Uterine spiral artery remodeling involves endothelial apoptosis induced by extravillous trophoblasts through Fas/FasL interactions. *Arterioscler Thromb Vasc Biol*. 2005;25(1):102–108.
54. Red-Horse K, et al. Cytotrophoblast induction of arterial apoptosis and lymphangiogenesis in an in vivo model of human placentation. *J Clin Invest*. 2006;116(10):2643–2652.
55. Leno-Durán E, et al. Human decidual stromal cells secrete soluble pro-apoptotic factors during decidualization in a cAMP-dependent manner. *Hum Reprod*. 2014;29(10):2269–2277.
56. Popovici RM, et al. Discovery of new inducible genes in in vitro decidualized human endometrial stromal cells using microarray technology. *Endocrinology*. 2000;141(9):3510–3513.
57. Walsh K, et al. Vascular cell apoptosis in remodeling, restenosis, and plaque rupture. *Circ Res*. 2000;87(3):184–188.
58. Lee MW, et al. The involvement of oxidative stress in tumor necrosis factor (TNF)-related apoptosis-inducing ligand (TRAIL)-induced apoptosis in HeLa cells. *Cancer Lett*. 2002;182(1):75–82.
59. Voltan R, et al. Redox signaling and oxidative stress: cross talk with TNF-related apoptosis inducing ligand activity. *Int J Biochem Cell Biol*. 2016;81(pt b):364–374.
60. Roberts JM, et al. Preeclampsia: an endothelial cell disorder. *Am J Obstet Gynecol*. 1989;161(5):1200–1204.
61. Lyall F. Priming and remodelling of human placental bed spiral arteries during pregnancy — a review. *Placenta*. 2005;26(suppl a):S31–S36.
62. Wang W, et al. Impaired sodium excretion and salt-sensitive hypertension in corin-deficient mice. *Kidney Int*. 2012;82(1):26–33.
63. Jiang J, et al. Ectodomain shedding and autocleavage of the cardiac membrane protease corin. *J Biol Chem*. 2011;286(12):10066–10072.